IEEE Access
Multidisciplinary | Rapid Review | Open Access Journal

Date of publication xxxx 00, 0000, date of current version xxxx 00, 0000.

Digital Object Identifier 10.1109/ACCESS.2017.DOI

A Hybrid Algorithm for Recognition of Power Quality Disturbances

RAJKUMAR KAUSHIK[1], OM PRAKASH MAHELA[2], (SENIOR MEMBER, IEEE), PRAMOD KUMAR BHATT[1], BASEEM KHAN[3], (MEMBER, IEEE), SANJEEVIKUMAR PADMANABHAN[4], (SENIOR MEMBER, IEEE), AND FREDE BLAABJERG [5], (FELLOW, IEEE)

[1]Department of Electrical Engineering, Amity University, Jaipur-303002, India (rajkaushik1812@gmail.com, pkbhatt@jpr.amity.edu)
[2]Power System Planning Division, Rajasthan Rajya Vidyut Prasaran Nigam Ltd., Jaipur-302005, India (opmahela@gmail.com)
[3]Department of Electrical Engineering, Hawassa University, Ethiopia (baseem.khan04@gmail.com)
[4]Centre for Biology and Green Engineering, Department of Energy Technology, Aalborg University, Esbjerg, Denmark (san@et.aau.dk)
[5]Villum Investigator and Professor of Power Electronics & Drives, Aalborg University, Esbjerg, Denmark (fbl@et.aau.dk)

Corresponding author: Baseem Khan (e-mail: baseem.khan04@gmail.com).

ABSTRACT An algorithm making use of hybrid features of Hilbert transform (HT) and Stockwell transform (ST) to identify the single-stage and multiple (multi-stage) power quality disturbances (PQDs) is introduced in this manuscript. A power quality index (PI) and time location index (TLI), based on the features computed from the voltage signal by the use of HT and ST are proposed for recognition of the PQDs. Four features extracted from the PI and TLI are considered for classification of the PQDs achieved using decision tree driven by rules. The algorithm is tested on the PQDs generated with the help of mathematical models (in conformity with standard IEEE-1159). Performance is evaluated on 100 data set of every disturbance computed by varying various parameters, and efficiency is found to be greater than 99%. It is established that an algorithm is effective for recognition of PQ events with an efficiency greater than 98% even in the presence of high-level noise. Algorithm is faster compared to many reported techniques and scalable for application to voltages of all range. Results are validated through comparison with the results of the algorithms reported in the literature. Performance of the algorithm is effectively validated on the practical utility network. This algorithm can be effectively implemented for designing the power quality (PQ) monitoring devices for the utility grids.

INDEX TERMS Hilbert transform, rule based decision tree, power quality disturbance, power quality index, Stockwell transform, time location index.

ABBREVIATIONS

DT	Decision tree
FCM	Fuzzy C-means clustering
GSS	Grid sub-station
HT	Hilbert transform
IEC	International Electro-technical Commission
IEEE	Institute of Electrical and Electronics Engineers
IT	Impulsive transient
LG	Line to ground fault
MAF	Maximum amplitude factor
MF	Median factor
MI	Momentary interruption
MN	Multiple notches
MS	Multiple spikes
OT	Oscillatory transient
PI	Power quality index
PP	Power plant
PQ	Power quality
PQD	Power quality disturbance
PSO	Particle swarm optimization
RBDT	Rule based decision tree
RE	Renewable energy
SF	Summation factor
SNR	Signal to noise ratio
ST	Stockwell transform
SVM	Support vector machine
TPP	Thermal power plant
TTT	Time-time transform

This article has been accepted for publication in a future issue of this journal, but has not been fully edited. Content may change prior to final publication. Citation information: DOI 10.1109/ACCESS.2020.3046425, IEEE Access

TLI Time location index

I. INTRODUCTION

THE utilities are aiming to feed good quality electric power to the loads continuously at an economical rate with high reliability. Disturbances such as swell, sag, momentary interruption (MI), harmonics, flicker, multiple spikes (MS), multiple notches (MN) and transients, which degrade the quality of the power are caused due to switching of heavy loads, use of power electronic loads (non-linear nature) and short circuits [1]. Hence, it becomes essential to identify the sources and causes of the PQDs, so that a mitigation action may be taken to supply good quality power to the customers. Methods and procedures, for identification and classification of the PQDs are defined in the standards, which include the IEEE-1159, the EN 50160 and the IEC 61000-4-30 [2]. Mathematical, smart signal processing and intelligent techniques play an important role in the identification and classification of the PQDs. Mahela *et al.* [3], presented a detailed study for the identification and classification of the PQDs and impact of noise on performance of the PQD recognition algorithms. This paper presented a detailed comparison between the different PQ recognition approaches, their suitability to identify a PQD, merits & demerits, limitations, computational complexity and effectiveness for implementation in PQ monitoring devices. A detailed comparative study of various techniques presented helps to select a method, which is the most effective for a particular application. A method using ST and time-time transform (TTT) for identification as well as feature extraction of the PQDs and ant colony optimization approach for classification of the PQDs is reported in [4]. This method achieved high accuracy by eliminating redundant features using a set of 15 synthetic signals of PQDs. A hybrid technique using Wavelet multiclass combined with the support vector machine (SVM) for identification and classification of the PQDs, simulated on practical power system network modelled IEEE-14 bus test system, is reported in [5]. This method is effective to reduce the processing time of the PQDs by simplifying the design architecture. Hooshmand *et al.* [6], introduced an approach using particle swarm optimization (PSO) and fuzzy logic for recognition of a set of 15 synthetic PQDs generated using mathematical models. This approach is effective for identification of the single and multiple PQDs with high accuracy and low computational burden. In [7], authors introduced a Stockwell transform supported method for recognition of the PQDs associated with operating events in the utility grid with penetration of wind energy. These events are emulated using a hardware set-up in the laboratory. Different operational events are rated in terms of power quality (PQ) using the proposed PQ index. Zhong *et al.* [8], designed an algorithm for identification of the PQDs using time-frequency evaluation and classification using decision tree supported rules. Algorithm tested on a set of 12 synthetic PQDs generated in MATLAB using mathematical models. This method gives better accuracy even in the presence of a noise level of 30-50dB signal to noise ratio (SNR). A technique for recognition of PQDs using ST based multi-resolution analysis and decision tree is reported in [9]. This method is validated by recognizing 16 synthetic PQDs generated in MATLAB using mathematical models. This method used adjustment factors for achieving controllable time-frequency resolution of the signals, which results in high accuracy of PQ detection. Lin *et al.* [10], introduced a technique for recognition of 8 kinds of synthetic PQDs using image enhancement approach and feature importance analysis. This method has merits of high accuracy, reduced number of redundant features and reduced computational complexity. The recognized PQDs can be mitigated using PQ improvement methods, and detection approaches help to initiate a suitable mitigation action. A detailed study on PQ mitigation method is available in [11].

A technique using ST based processing of the voltage signal to recognize both the single-stage and multiple PQDs is reported in [12] and [13] respectively, where the classification of the PQDs is achieved using RBDT. This technique is effective to identify the PQDs having transient-nature such as oscillatory transient (OT) and impulsive transient (IT) with high accuracy. However, this method is less effective to identify the PQDs related to amplitude. A technique using HT based processing of voltage signal with both single-stage and multiple PQDs is reported in [14] and [15] respectively, where the classification of the PQDs is achieved using rule based decision tree (RBDT). This technique is effective for identifying the amplitude-related PQDs such as sag, swell, MI, MS and MN. However, this is less effective for identifying the transient-related PQDs. Hence, this paper is aimed to design a hybrid algorithm, which combines the merits of both the HT and ST algorithms. This helps to detect all the PQDs related to the amplitude, transients and frequency with high accuracy. Main contributions of this paper are as follows:

- An algorithm making use of a hybrid combination of the features of voltage signal computed using the Hilbert transform and Stockwell transform is proposed. This method is effective to identify both the single-stage (one disturbance at a time) and multiple (two or more disturbances at a time) PQDs. This is achieved by keeping the number of features to the minimum.
- Both the single-stage and multiple PQDs are classified using the RBDT. This is achieved with high efficiency greater than 99% by the use of features of PQDs, extracted using HT and ST.
- Performance of the algorithm is least affected by the availability of noise.
- Algorithm performs better compared to the ST & RBDT algorithm, ST & DT + FCM (Fuzzy C-means clustering) and HT & RBDT algorithm.
- This approach has the low computational complexity.
- Algorithm has scalability for application to voltages of all range.

All contents in the paper are divided into eight sections. The introductory part is included in Section I. Generation of

the single-stage, and multiple PQDs is detailed in Section II. It also describes the proposed algorithm used for recognition of PQDs. Simulation results describing the identification of the PQDs are detailed and discussed in Section III, whereas the classification results of the PQDs are included in Section IV. Performance computation of the proposed algorithm is included in Section V. Section VI illustrates the results to establish the suitability of the algorithm to recognize the PQDs associated with the practical power system network. A comparative study between the performance of the proposed algorithm and algorithms reported in the literature is included in Section VII. Detailed results for analysis of effect of noise on performance and computational complexity of algorithm are also discussed in this Section. The concluding remark of the algorithm is incorporated in Section VIII.

II. GENERATION OF PQDS AND PROPOSED ALGORITHM

This section describes the generation of the PQDs and algorithm designed for detection and classification of these disturbances. Mathematical and signal processing tools utilized for designing the proposed algorithm are also detailed in this section.

A. GENERATION OF PQ DISTURBANCES

Signals having a power frequency of 50 Hz with superimposed single-stage PQDs are generated in MATLAB software with the help of mathematical formulation. These PQDs are generated in conformity with IEEE-1159 standard using models reported in [16], [17]. These signals are used to establish the performance of the algorithm. Mathematical equations of voltage signals with single-stage PQDs, standard parameters and their simulated values are tabulated in Table 1 [17]. In this table symbol, PQD1 represents the voltage signal without any disturbance. The symbols PQD2 to PQD10 are used to represent the single-stage PQ disturbances where only one disturbance is associated with the signal. Multiple PQDs are generated by various combinations of mathematical equations of single-stage PQDs as detailed in Table 1 [17]. The combination of single-stage PQDs formulates multiple PQDs (two or more PQDs are associated with the signal). The mathematical formulation, standard parameters and simulated parameters of multiple PQDs are tabulated in Table 2, where simulated values are also represented. In this table, symbols PQD11 to PQD12 are used to represent the multiple PQDs.

B. PROPOSED ALGORITHM

A block scheme of the algorithm proposed for recognition of the PQDs is described in Fig. 1. This algorithm is based on the use of features of the voltage signal extracted using the Hilbert transform and Stockwell transform. Per unit values of the voltage signal are used by this algorithm and PQ issues are investigated using distortions in the voltage signals from the standard pure sinusoidal nature, magnitude from unity and frequency from the standard value of 50 Hz. Hence, this algorithm has scalability for application to voltages of all range. Further, tuning procedure is not required for the parameters and features used by the algorithm because algorithm uses deviations of parameters from standard values.

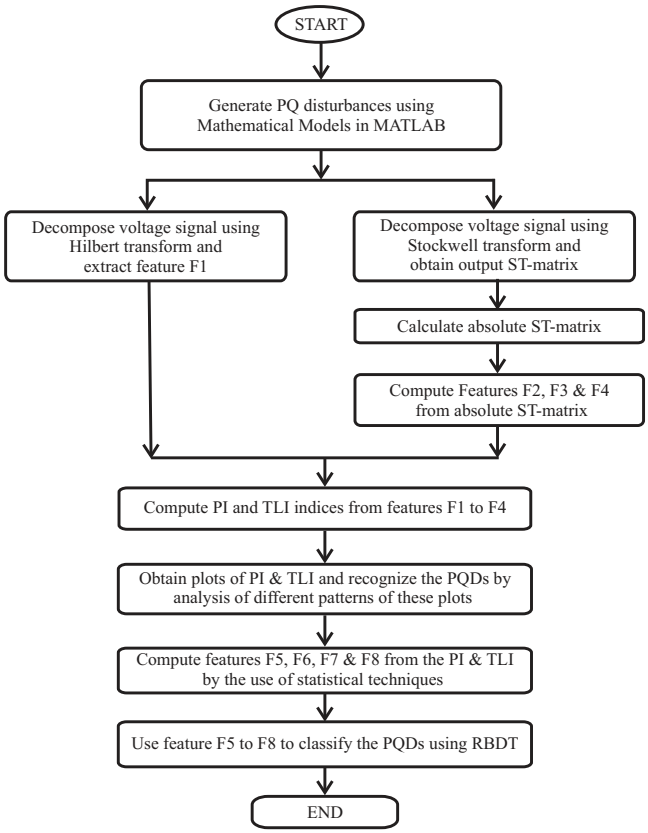

FIGURE 1. Hybrid algorithm for recognition of PQ disturbances

The voltage signals with PQDs are sampled at a sampling frequency of 3.2 kHz (64 samples per cycle) for a period of 10 cycles. The Hilbert transform (HT) is used for processing the PQDs. This helps in the computation of the momentary frequencies, as well as amplitudes, which can be used for description of the signal. The mathematical formulation reported in [18] is used for HT based decomposition of a voltage signal with PQD. The HT gives instantaneous physical frequencies for the special class of function. As an example, functions having non-zero mean values will results in negative frequency contributions with the help of HT. Hence, signals analysed with the help of HT should be restricted in such a manner that evaluated instantaneous frequency functions should have physical meaning [18]. The voltage signals with PQDs are decomposed using Hilbert transform, and absolute values of output are evaluated and designated as Feature F1, which is described below.

$$F1 = abs(hilbert(S)) \tag{1}$$

Voltage signal with PQDs is also decomposed using multi-resolution analysis of ST at a sampling frequency of $3.2kHz$ and S-matrix is computed, which gives time-frequency representation of the signal. ST is effective to extract information

This article has been accepted for publication in a future issue of this journal, but has not been fully edited. Content may change prior to final publication. Citation information: DOI 10.1109/ACCESS.2020.3046425, IEEE Access

TABLE 1. Mathematical Modeling of Simulated single stage PQ Disturbances

PQ	Symbol of PQD	Mathematical model	Parameters of PQ Disturbances	
			As per Standard	Used in Simulation
Voltage without PQD	PQD1	$V(t) = Asin(\omega t)$	$\omega = 2\pi f$	$A = 1pu, f = 50Hz$
Voltage with sag	PQD2	$V(t) = (1 - \alpha(u(t-t_1) - u(t-t_2)))sin(\omega t)$	$0.1 \leq \alpha \leq 0.9, T \leq t_2 - t_1 \leq 9T$	$\alpha = 0.3, t_1 = 0.06, t_2 = 0.14$
Voltage with swell	PQD3	$V(t) = (1 + \alpha(u(t-t_1) - u(t-t_2)))sin(\omega t)$	$0.1 \leq \alpha \leq 0.8, T \leq t_2 - t_1 \leq 9T$	$\alpha = 0.3, t_1 = 0.06, t_2 = 0.14$
Voltage with MI	PQD4	$V(t) = (1 - \alpha(u(t-t_1) - u(t-t_2)))sin(\omega t)$	$0.9 \leq \alpha \leq 1.0, T \leq t_2 - t_1 \leq 9T$	$\alpha = 0.95, t_1 = 0.06, t_2 = 0.14$
Voltage with Flicker	PQD5	$V(t) = (1 + \alpha_f sin(\beta\omega t))sin(\omega t)$	$0.1 \leq \alpha_f \leq 0.2, 5 \leq \beta \leq 20Hz$	$\alpha_f = 0.15, \beta = 15$
Voltage with OT	PQD6	$V(t) = sin(\omega t) + \alpha e^{\frac{(t-t_1)}{\tau}} sin\omega_n(t-t_1)\{u(t_2 - u(t_1))\}$	$0.1 \leq \alpha \leq 0.8, 0.05T \leq t_2 - t_1 \leq 3T, 8ms \leq \tau \leq 40ms, 300 \leq f_n \leq 900Hz$	$\alpha = 0.8, t_1 = 0.08, \tau = 0.02, t_2 = 0.10$
Voltage with IT	PQD7	$V(t) = sin(\omega t) + \alpha e^{\frac{(t-t_1)}{\tau}} - \alpha e^{\frac{(t-t_1)}{\tau}}\{u(t_2 - u(t_1))\}$	$1 \leq \alpha \leq 10, 0.05T \leq t_2 - t_1 \leq 3T, 8ms \leq \tau \leq 40ms$	$\alpha = 10, t_1 = 0.085, \tau = 0.02, t_2 = 0.088$
Voltage with Harmonics	PQD8	$V(t) = \alpha_1 sin(\omega t) + \alpha_3 sin(3\omega t) + \alpha_5 sin(5\omega t) + \alpha_7 sin(7\omega t)$	$0.1 \leq \alpha_3, \alpha_5, \alpha_7 \leq 0.15$	$\alpha_3 = 0.05, \alpha_5 = 0.10, \alpha_7 = 0.15$
Voltage with MN	PQD9	$V(t) = sin(\omega t) - sign(sin(\omega t)) \times \left[\sum_{n=0}^{9} K \times \{u(t - (t_1 + 0.02n)) - u(t - (t_2 + 0.02n))\}\right]$	$0.1 \leq K \leq 0.4, 0 \leq t_1, t_2 \leq 0.5T, 0.01T \leq t_2 - t_1 \leq 0.05T$	$K = 0.4, t_1 = 0.006, t_2 = 0.0065$
Voltage with MS	PQD10	$V(t) = sin(\omega t) + sign(sin(\omega t)) \times \left[\sum_{n=0}^{9} K \times \{u(t - (t_1 + 0.02n)) - u(t - (t_2 + 0.02n))\}\right]$	$0.1 \leq K \leq 0.4, 0 \leq t_1, t_2 \leq 0.5T, 0.01T \leq t_2 - t_1 \leq 0.05T$	$K = 0.4, t_1 = 0.002, t_2 = 0.0023$

A: amplitude; f: frequency; V: voltage; T: time period; τ: time constant; ω: angular frequency; u(t): unit step function

TABLE 2. Mathematical Modeling of Simulated multiple PQ Disturbances

PQ	Symbol of PQD	Mathematical model	Parameters of PQD	
			As per Standard	Used in Simulation
Voltage with sag & harmonics	PQD11	$V(t) = (1-\alpha(u(t-t_1)-u(t-t_2)))sin(\omega t)+\alpha_3 sin(\omega t)+\alpha_5 sin(\omega t)+\alpha_7 sin(\omega t)$	$\omega = 2\pi f; 0.1 \leq \alpha \leq 0.9, T \leq t_2 - t_1 \leq 9T; 0.1 \leq \alpha_3, \alpha_5, \alpha_7 \leq 0.15$	$f = 50Hz; \alpha = 0.3, t_1 = 0.06, t_2 = 0.14; \alpha_3 = 0.05, \alpha_5 = 0.10, \alpha_7 = 0.15$
Voltage with flicker & harmonics	PQD12	$V(t) = (1+\alpha_f sin(\beta\omega t))sin(\omega t)+\alpha_3 sin(\omega t)+\alpha_5 sin(\omega t)+\alpha_7 sin(\omega t)$	$0.1 \leq \alpha_f \leq 0.2, 5 \leq \beta \leq 20Hz; 0.1 \leq \alpha_3, \alpha_5, \alpha_7 \leq 0.15$	$\alpha_f = 0.15, \beta = 15; \alpha_3 = 0.05, \alpha_5 = 0.10, \alpha_7 = 0.15$
Voltage with flicker & OT	PQD13	$V(t) = (1 + \alpha_f sin(\beta\omega t))sin(\omega t) + \alpha e^{\frac{(t-t_1)}{\tau}} sin\omega_n(t-t_1)\{u(t_2 - u(t_1))\}$	$0.1 \leq \alpha_f \leq 0.2, 5 \leq \beta \leq 20Hz; 0.1 \leq \alpha \leq 0.8, 0.05T \leq t_2 - t_1 \leq 3T, 8ms \leq \tau \leq 40ms, 300 \leq f_n \leq 900Hz$	$\alpha_f = 0.15, \beta = 15; \alpha = 0.8, t_1 = 0.08, \tau = 0.02, t_2 = 0.10, f_n = 400Hz$
Voltage with harmonics & IT	PQD14	$V(t) = sin(\omega t) + \alpha_3 sin(\omega t) + \alpha_5 sin(\omega t) + \alpha_7 sin(\omega t) + \alpha e^{\frac{(t-t_1)}{\tau}} - \alpha e^{\frac{(t-t_1)}{\tau}}\{u(t_2 - u(t_1))\}$	$0.1 \leq \alpha_3, \alpha_5, \alpha_7 \leq 0.15; 1 \leq \alpha \leq 10, 0.05T \leq t_2 - t_1 \leq 3T, 8ms \leq \tau \leq 40ms$	$\alpha_3 = 0.05, \alpha_5 = 0.10, \alpha_7 = 0.15; \alpha = 10, t_1 = 0.085, \tau = 0.02, t_2 = 0.088$
Voltage with MS & sag	PQD15	$V(t) = (1 - \alpha(u(t-t_1) - u(t-t_2)))sin(\omega t) + sign(sin(\omega t)) \times \left[\sum_{n=0}^{9} K \times \{u(t - (t_3 + 0.02n)) - u(t - (t_4 + 0.02n))\}\right]$	$0.1 \leq \alpha \leq 0.9, T \leq t_2 - t_1 \leq 9T; 0.1 \leq K \leq 0.4, 0 \leq t_3, t_4 \leq 0.5T, 0.01T \leq t_4 - t_3 \leq 0.05T$	$\alpha = 0.3, t_1 = 0.06, t_2 = 0.14; K = 0.4, t_3 = 0.002, t_4 = 0.0023$
Voltage with OT, sag, harmonics & IT	PQD16	$V(t) = (1 - \alpha_1(u(t-t_1) - u(t-t_2)))sin(\omega t) + \alpha_2 e^{\frac{(t-t_3)}{\tau_1}} sin\omega_n(t - t_3)\{u(t_4 - u(t_3))\} + \alpha_3 sin(\omega t) + \alpha_5 sin(\omega t) + \alpha_7 sin(\omega t) + \beta e^{\frac{(t-t_5)}{\tau_2}} - \beta e^{\frac{(t-t_5)}{\tau_2}}\{u(t_6 - u(t_5))\}$	$0.1 \leq \alpha_1 \leq 0.9, T \leq t_2 - t_1 \leq 9T; 0.1 \leq \alpha_2 \leq 0.8, 0.05T \leq t_4 - t_3 \leq 3T, 8ms \leq \tau_1 \leq 40ms, 300 \leq f_n \leq 900Hz; 0.1 \leq \alpha_3, \alpha_5, \alpha_7 \leq 0.15; 1 \leq \beta \leq 10, 0.05T \leq t_6 - t_5 \leq 3T, 8ms \leq \tau_2 \leq 40ms$	$\alpha_1 = 0.3, t_1 = 0.06, t_2 = 0.14; \alpha_2 = 0.8, t_3 = 0.09, \tau_1 = 0.02, t_4 = 0.11, f_n = 400Hz; \alpha_3 = 0.05, \alpha_5 = 0.10, \alpha_7 = 0.15; \beta = 10, t_5 = 0.098, \tau_2 = 0.02, t_6 = 0.101$

A: amplitude; f: frequency; V: voltage; T: time period; τ: time constant; ω: angular frequency; u(t): unit step function

of both the phase and amplitude of the spectrum. The output of ST is obtained in the form of a complex matrix which is represented as S-matrix. Each row element in this matrix corresponds to a frequency, and each column corresponds to a time instant. Matrix of ST-amplitude (STA) is formed from absolute values of this S-matrix. ST is utilized with the help of a multi-resolution based on window width, which is changing inversely proportional to the frequency and power data changing with time. Hence, a great resolution of time at a high frequency and a low time resolution at a low frequency are achieved. There are different methods of achieving the ST [19]. If the window of ST is wide in the time domain, the ST can be used to provide high resolution of frequency when lower frequency components are present in the signal. Similarly, the window is narrow for achieving good time resolution at the moments of high-frequency components available with the signal. Information related to the frequency and amplitude of the signal can be derived from the S-matrix [20], [21]. The features F2, F3 and F4, have been extracted from this matrix which is used to define the PI and TLI. Features F2 to F4 are extracted from this matrix and described as below:

F2: Summation factor (SF). It is computed using the summation of each column of the S-matrix.

$$F2 = sum(abs(S - matrix)) \tag{2}$$

F3: Maximum amplitude factor (MAF). It represents the maximum amplitude in each column of the S-matrix.

$$F3 = max(abs(S - matrix)) \tag{3}$$

F4: Median factor (MF). It represents the median of the S-matrix concerning columns.

$$F4 = median(abs(S - matrix)) \tag{4}$$

1) Power Quality Index

A power quality index (PI) is introduced to detect various PQDs. It is computed by multiplying the features F1, F2 and F3 sample by sample as detailed below:

$$PI = abs(F1. * F2. * F3) \tag{5}$$

This index is plotted for a period of 10 cycles of PQDs. Patterns of these plots are utilized to identify all the investigated PQDs. This index is effective to recognize all types of disturbances. However, its performance might be limited for disturbances of low frequency and low magnitude. This limitation can be overcome by combining the patterns of time location index (TLI).

2) Time Location Index

An index is introduced to localize the PQ events with respect to time and designated as the time location index (TLI). This is computed by multiplying the features F1, F2, F3 and F4 sample by sample. TLI is detailed below.

$$TLI = (F1. * F2. * F3. * F4). * (1000); \quad (6)$$

Here a weight factor of 1000 is used to obtain results with the high resolution because feature F4 has an additive advantage of detecting the patterns observed at the time of initiation and end of a PQD, but its magnitude is low. Hence, the weight factor helps to increase the magnitude of TLI for clear visibility. Further, this value of weight factor for TLI effectively detects all the types of PQ disturbances in a real-time network of the utility grid and can be used universally. During a healthy condition, the TLI has nearly zero value and a non-zero value for the incidence of a PQ disturbance. The TLI is plotted for a period of 10 cycles. Analysis of the patterns of TLI indicates the location of PQDs. This index is also effective to identify high-frequency PQDs. The index effectively localizes the voltage magnitude related to PQDs. However, multiple spikes are observed for frequency-dependent PQDs. This limitation is overcome if patterns of PI and TLI are used together to recognize the PQDs. This index might be useful for recognition of the operational events such as islanding, outage of renewable energy (RE) generators and grid synchronization of RE generators. This will be considered as future scope of work.

C. CLASSIFICATION OF PQDS

The classification of the PQDs is achieved using the rules supported by a decision tree. The rule-based decision tree (RBDT) was introduced by the Breiman in 1980 and applied in the field of power system by the Wehenkel in 1989. In this technique, decision supported rules are used for classification of PQ disturbances to predict the data responses. For achieve this, decisions are followed in the form of a tree starting from the root (starting point) node to a leaf node (final decision node). Hence, the leaf node has the final decision of classification. This classification tree is effective for giving a response which is effective and nominal and can be implemented using the 'true' or 'false' decision technique. Hence, it is supported by a set of rules which can be applied to a set of data containing the features of signals with PQ disturbances [22]. Features F5-F8 are used as input to the decision tree to obtain results for classification of the PQDs. The features F5 & F6 are computed from the PI plot by calculating its variance and median, respectively. Similarly, the features F7 & F8 are computed from the TLI plot by calculating its variance and median, respectively. These features are considered as input to the rule-based decision tree (RBDT) for classifying the PQDs. RBDT has the merit of low computational burden due to its single-stage and requirement of fewer data. These are calculated as detailed below:

F5: It represents the variance of PI plot.

$$F5 = var(PI) \quad (7)$$

F6: It represents the median of PI plot.

$$F6 = median(PI) \quad (8)$$

F7: It represents the variance of TLI plot.

$$F7 = var(TLI) \quad (9)$$

F8: It represents the median of TLI plot.

$$F8 = median(TLI) \quad (10)$$

Performance of the algorithm is tested on 100 sets of data for each PQD computed by varying the parameters like magnitude, time of incidence of PQD, and frequency of PQD, frequency of the voltage signal (50 Hz and 60 Hz). Performance is also tested in a noisy environment by considering a noise level of 20 dB SNR. This algorithm is effective for implementation in the online PQ monitoring devices.

III. DETECTION OF PQ EVENTS: SIMULATION RESULTS

This section details the analysis of PQDs using the algorithm proposed in this paper. The PI and TLI plots obtained with the help of features F1 to F4 are used for detection of the PQDs. These plots pertaining to the pure sine wave are considered as a reference curve for detection and localization of the PQDs. Patterns of the PI and TLI plots are effective to identify the parameters associated with the disturbances such as magnitude of sag, swell, MI, OT, IT etc. Further, the frequency components associated with the disturbances can also be recognized using the patterns of PI and TLI plots. Detailed results are discussed in the following sections.

A. VOLTAGE SIGNAL WITHOUT PQ DISTURBANCE

The voltage signal of a sine wave for a period of 10 cycles, PI and TLI plots are illustrated in Fig. 2 and these plots are considered as a reference for detecting the PQDs. Fig. 2 (a) illustrates the pure sine wave where any PQD is not visible. Fig. 2 (b) indicates that amplitude of the PI plot is constant at unity value. In the presence of PQD associated with the sine wave, magnitude of the PI plot either increase, or decrease depending on the type of PQD. It is inferred from Fig. 2 (c) that TLI plot also has constant magnitude with zero value. At the moment of deviation of the waveform from pure sinusoidal nature, the magnitude of TLI becomes high, which indicates the incidence of a PQD. Hence, it is established that PQD is not associated with the voltage signal.

This article has been accepted for publication in a future issue of this journal, but has not been fully edited. Content may change prior to final publication. Citation information: DOI 10.1109/ACCESS.2020.3046425, IEEE Access

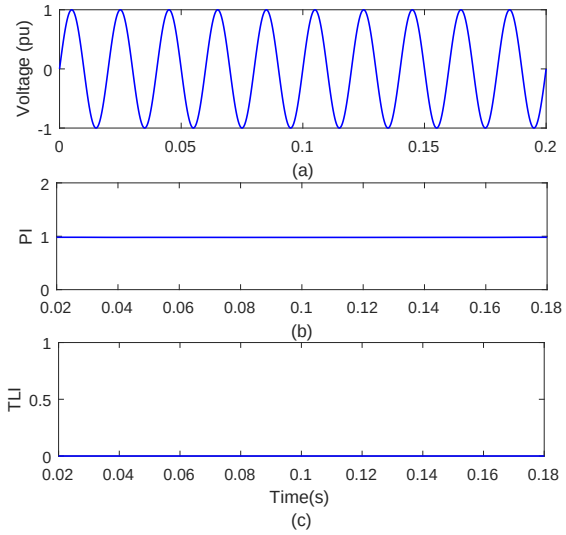

FIGURE 2. Voltage signal without PQ disturbance (a) voltage signal (b) power quality index (c) time location index

B. VOLTAGE SIGNAL WITH SAG

The voltage signal of a sine wave with sag for a period of 10 cycles, PI and TLI plots are illustrated in Fig. 3. Fig. 3 (a) indicates that sine wave has a superimposed sag between $0.06s$ to $0.14s$. Fig. 3 (b) indicates that amplitude of the PI plot has decreased at $0.06s$ and again regains the original value at $0.14s$. This effectively detects the sag associated with the voltage signal. Fig. 3 (c) indicates that the TLI plot has zero magnitudes except at $0.06s$ (incidence of sag) and $0.14s$ (end of sag) where there are sharp magnitude peaks. These sharp magnitude peaks effectively localizes the voltage sag. Hence, patterns of PI and TLI plots when combined together, effectively identify and localize the sag associated with the voltage signal.

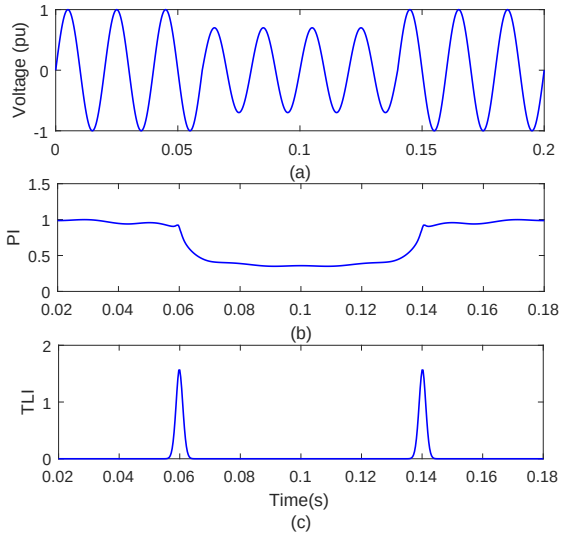

FIGURE 3. Voltage signal with sag disturbance (a) voltage signal (b) power quality index (c) time location index

Gaussian noise of 10 dB SNR is superimposed on the voltage signal of a sine wave with sag for a period of 10 cycles. Voltage signal with sag and noise, PI and TLI plots are illustrated in Fig. 4. Fig. 4 (a) indicates that voltage sag between $0.06s$ to $0.14s$ and noise is observed over the entire signal period. Fig. 4 (b) indicates that amplitude of the PI plot has decreased at $0.06s$ and again regains the original value at $0.14s$. However, small magnitude ripples are observed over entire time range due to noise component. This effectively detects the sag associated with the voltage signal in noisy environment. Fig. 4 (c) indicates that the TLI plot has ripples over entire time period of signal due to available noise. However, peak magnitudes of high magnitude are observed at $0.06s$ (incidence of sag) and $0.14s$ (end of sag) indicating the start and end of the sag in voltage. Hence, patterns of PI and TLI plots when combined together, effectively identified and localized the sag associated with the voltage signal in the presence of Gaussian noise of 10 dB SNR. Further, in the presence of noise level higher than 10 dB SNR, voltage sag has not been recognized effectively.

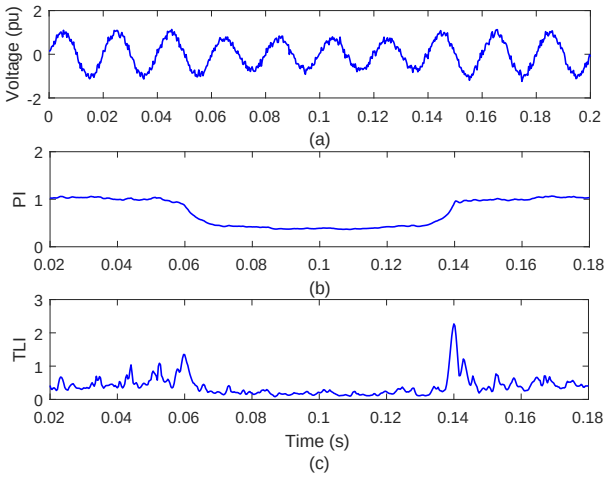

FIGURE 4. Voltage signal with sag disturbance in noisy environment (10 dB SNR) (a) voltage signal (b) power quality index (c) time location index

C. VOLTAGE SIGNAL WITH SWELL

The voltage signal of a sine wave with swell for a period of 10 cycles, PI and TLI plots are illustrated in Fig. 5. Fig. 5 (a) indicates that sine wave has a superimposed swell between $0.06s$ to $0.14s$. Fig. 5 (b) indicates that amplitude of the PI plot has increased at $0.06s$ and again regains the original value at $0.14s$. This effectively detects the swell associated with the voltage signal. Fig. 5 (c) indicates that TLI plot has zero magnitudes except at $0.06s$ (incidence of swell) and $0.14s$ (end of swell) where there are sharp magnitude peaks. These sharp magnitude peaks effectively localize the voltage swell. Hence, patterns of PI and TLI plots when combined together, effectively identify and localize the swell associated with the voltage signal.

This article has been accepted for publication in a future issue of this journal, but has not been fully edited. Content may change prior to final publication. Citation information: DOI 10.1109/ACCESS.2020.3046425, IEEE Access

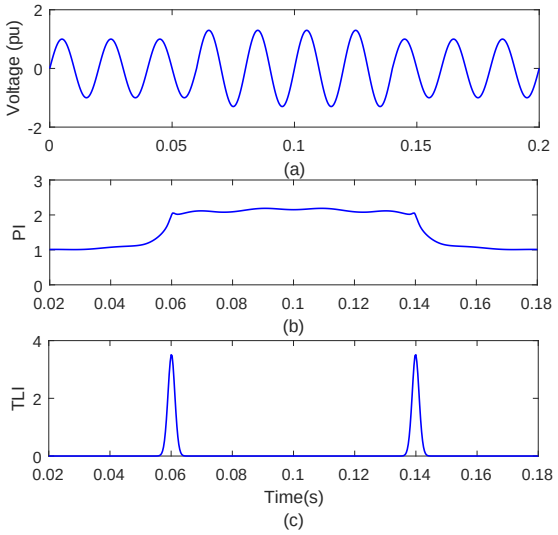

FIGURE 5. Voltage signal with swell disturbance (a) voltage signal (b) power quality index (c) time location index

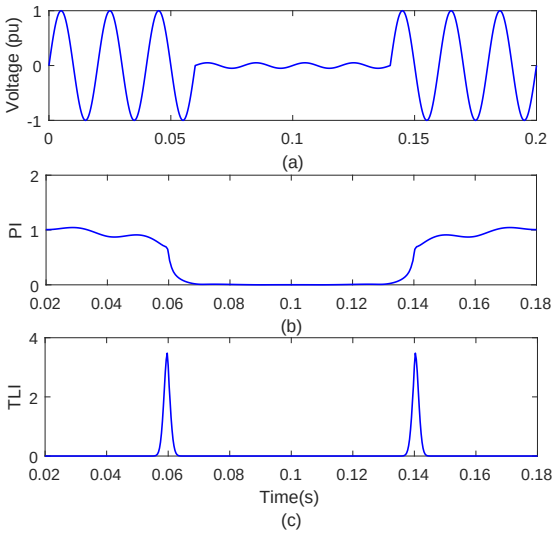

FIGURE 6. Voltage signal with momentary interruption disturbance (a) voltage signal (b) power quality index (c) time location index

D. VOLTAGE SIGNAL WITH MOMENTARY INTERRUPTION

The voltage signal of a sine wave with momentary interruption (MI) for a period of 10 cycles, PI and TLI plots are illustrated in Fig. 6. Fig. 6 (a) indicates that sine wave has a superimposed MI between $0.06s$ to $0.14s$. Fig. 6 (b) indicates that amplitude of the PI plot has decreased to shallow values (below 10%) at $0.06s$ and again regains the original value at $0.14s$. This effectively detects the MI associated with the voltage signal. Fig. 6 (c) indicates that the TLI plot has zero magnitudes except at $0.06s$ (incidence of MI) and $0.14s$ (end of MI) where there are sharp magnitude peaks. These sharp magnitude peaks effectively localize the momentary interruption. Hence, patterns of PI and TLI plots when combined together, effectively identify and localize the MI associated with the voltage signal.

E. VOLTAGE SIGNAL WITH HARMONICS

The voltage signal of a sine wave with superimposed 3^{rd}, 5^{th} & 7^{th} harmonics for a period of 10 cycles, PI and TLI plots are illustrated in Fig. 7. Fig. 7 (a) indicates the sine wave with superimposed 3^{rd}, 5^{th} & 7^{th} harmonics. Fig. 7 (b) indicates that there are ripples with regular pattern over entire time range which effectively detects the harmonics associated with the voltage signal. Fig. 7 (c) indicates that the TLI plot also has ripples with regular pattern over entire time range which effectively detect the harmonics associated with the voltage signal. Here, both the PI and TLI plots effectively detects the harmonics superimposed over the voltage signal.

F. VOLTAGE SIGNAL WITH FLICKER

The voltage signal of a sine wave with superimposed flicker for a period of 10 cycles, PI and TLI plots are illustrated in Fig. 8. Fig. 8 (a) indicates the sine wave with superimposed flicker. Fig. 8 (b) indicates that magnitude has increased and

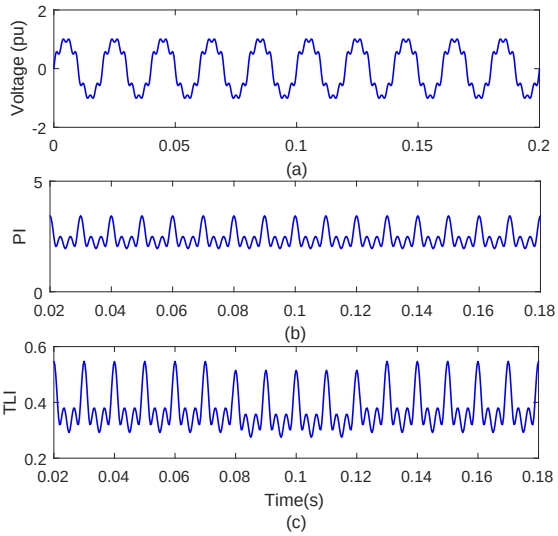

FIGURE 7. Voltage signal with harmonics disturbance (a) voltage signal (b) power quality index (c) time location index

becomes greater than the standard value of $1pu$ following the regular pattern of crest and trough with ripples superimposed on the crest. This specific pattern associated with the PI plot effectively detects the presence of flicker superimposed on the signal. Similarly, the Fig. 8 (c) also indicates that magnitude has increased and becomes greater than the standard value for a sine wave following the regular pattern of crest and trough with flicker superimposed on the crest. This specific pattern associated with the TLI plot effectively detects the presence of ripples superimposed on the signal. Here, both the PI and TLI plots effectively detect the flicker superimposed over the voltage signal.

This article has been accepted for publication in a future issue of this journal, but has not been fully edited. Content may change prior to final publication. Citation information: DOI 10.1109/ACCESS.2020.3046425, IEEE Access

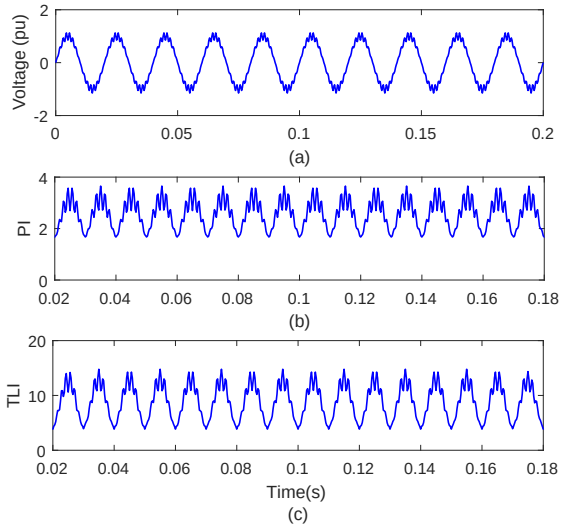

FIGURE 8. Voltage signal with flicker disturbance (a) voltage signal (b) power quality index (c) time location index

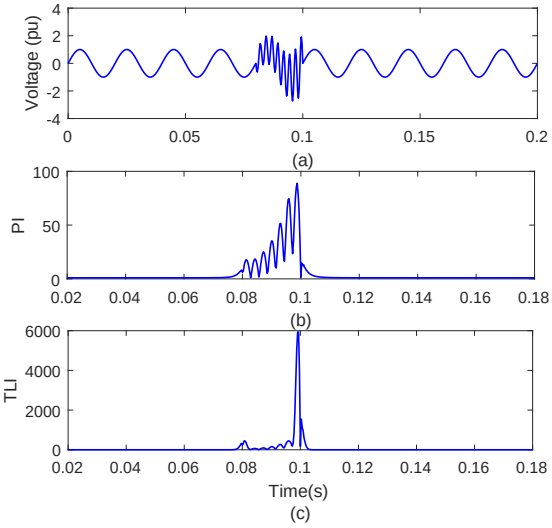

FIGURE 9. Voltage signal with oscillatory transient disturbance (a) voltage signal (b) power quality index (c) time location index

G. VOLTAGE SIGNAL WITH OSCILLATORY TRANSIENT

The voltage signal of a sine wave with superimposed OT for a period of 10 cycles, PI and TLI plots are illustrated in Fig. 9. Fig. 9 (a) indicates the sine wave with superimposed OT between $0.08s$ to $0.10s$. Fig. 9 (b) indicates that high magnitude has been observed between $0.08s$ to $0.10s$ with continuously increasing magnitude from $0.08s$ to $0.10s$ where the continuous pattern of ripples is available on the upper surface of the PI plot. This specific pattern associated with the PI plot effectively detects the presence of OT superimposed on the signal. Fig. 9 (c) indicates that sharp magnitude peaks are associated with the TLI plot at $0.06s$ (incidence of OT) and $0.14s$ (end of OT) which effectively localize the OT. Hence, patterns of PI and TLI plots when combined, effectively identify and localize the OT associated with the voltage signal.

H. VOLTAGE SIGNAL WITH IMPULSIVE TRANSIENT

The voltage signal with superimposed IT for a period of 10 cycles, PI and TLI plots are illustrated in Fig. 10. Fig. 10 (a) indicates that sine wave has a superimposed OT between $0.085s$ to $0.088s$. Fig. 10 (b) indicates that the sharp peak of very high magnitude has been observed between $0.085s$ to $0.088s$. This very high magnitude peak effectively detects the presence of IT superimposed on the signal. Similarly, Fig. 10 (c) indicates that sharp peak of very high magnitude has been observed with the TLI plot between $0.085s$ to $0.088s$ which helps to effectively localize the IT. Hence, it is established that the rise time and fall time of the disturbances have been tracked by the PI and TLI plots in the same way as it is in the actual signal. There is no delay in the tracking of rising time and fall time of the disturbances. Further, the speed of response in PI and TLI plots is similar to the actual disturbance. Hence, the speed of response cannot be adjusted.

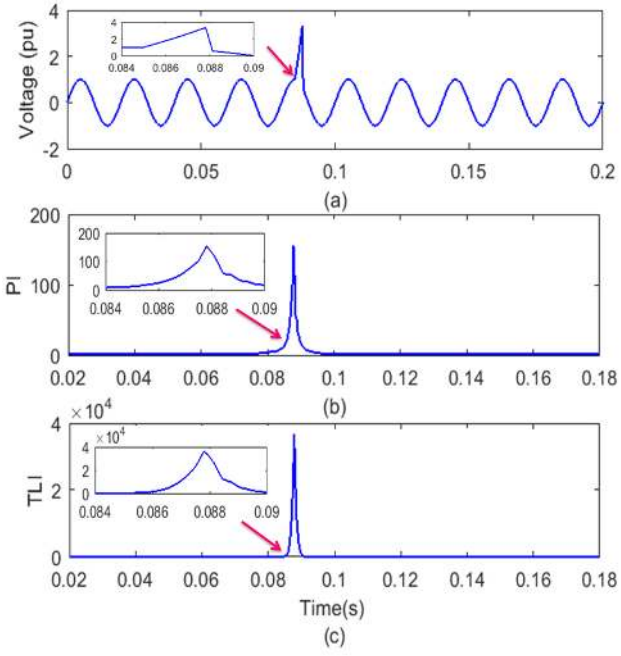

FIGURE 10. Voltage signal with impulsive transient disturbance (a) voltage signal (b) power quality index (c) time location index

I. VOLTAGE SIGNAL WITH MULTIPLE NOTCHES

The voltage signal with MN for a period of 10 cycles, PI and TLI plots are illustrated in Fig. 11. Fig. 11 (a) indicates that the sine wave has a superimposed MN with a regular pattern. Fig. 11 (b) indicates that a series of regularly spaced sharp peaks with two peaks at the top surface is present. This specific pattern, with two peaks pattern associated with the high magnitude peaks, effectively detects the presence of MN superimposed on the signal. Fig. 11 (c) also indicates that a series of regularly spaced sharp peaks, with two peaks

This article has been accepted for publication in a future issue of this journal, but has not been fully edited. Content may change prior to final publication. Citation information: DOI 10.1109/ACCESS.2020.3046425, IEEE Access

at the top surface, is present. However, rise and decay time for these peaks are lower compared to the peaks observed in the PI plot. This specific pattern, with two peaks pattern associated with the high magnitude peaks, effectively detects the presence of MN superimposed on the signal.

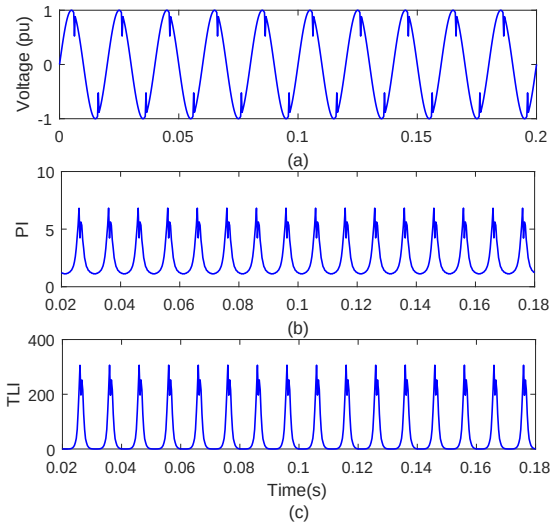

FIGURE 11. Voltage signal with multiple notches disturbance (a) voltage signal (b) power quality index (c) time location index

J. VOLTAGE SIGNAL WITH MULTIPLE SPIKES

The voltage signal with MS for a period of 10 cycles, PI and TLI plots are illustrated in Fig. 12. Fig. 12 (a) indicates that the sine wave with superimposed MS with the regular pattern. Fig. 12 (b) indicates that a series of regularly spaced sharp peaks with a single peak at the top surface is present. This specific pattern, with single peak pattern associated with the high magnitude peaks, effectively detects the presence of MS superimposed on the signal and also discriminated from the MN. Fig. 12 (c) also indicates that a series of regularly spaced sharp peaks with a single peak at the top surface is present. However, rise and decay time for these peaks are lower compared to the peaks observed in the PI plot. This specific pattern, with single peak pattern associated with the high magnitude peaks, effectively detects the presence of MS superimposed on the signal and also distinguished from the MN.

K. VOLTAGE SIGNAL WITH SAG AND HARMONICS

The voltage signal of a sine wave with superimposed sag and 3^{rd}, 5^{th} & 7^{th} harmonics for a period of 10 cycles, PI and TLI plots are illustrated in Fig. 13. Fig. 13 (a) indicates the sine wave with superimposed 3^{rd}, 5^{th} & 7^{th} harmonics with regular pattern and sag between $0.06s$ to $0.14s$. Fig. 13 (b) indicates that amplitude of the PI plot has decreased at $0.06s$ and again regains the original value at $0.14s$, which detects the sag. Further, the ripples with the regular pattern observed over the entire time range of PI plot effectively detect the harmonics. Hence, multiple PQ disturbance of sag

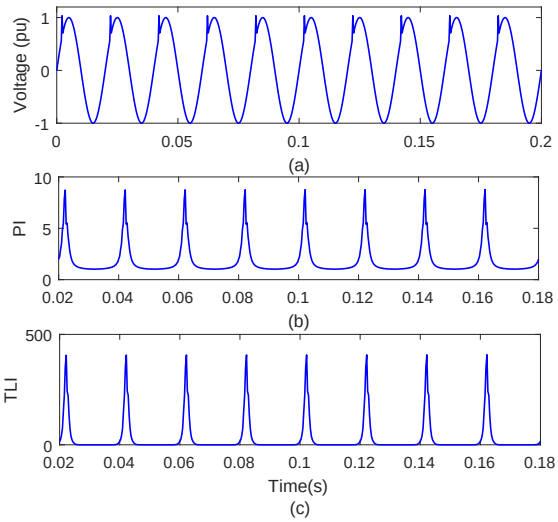

FIGURE 12. Voltage signal with multiple spikes disturbance (a) voltage signal (b) power quality index (c) time location index

and harmonics associated with the voltage signal has been detected effectively.

Fig. 13 (c) indicates that the TLI plot has zero magnitudes except at $0.06s$ (incidence of sag) and $0.14s$ (end of sag) where there are sharp magnitude peaks. These sharp magnitude peaks effectively localize the voltage sag. Further, Fig. 13 (c) indicates that the TLI plot also has ripples with the regular pattern over the entire time range, which effectively detects the harmonics associated with the voltage signal. Hence, multiple PQ disturbance of sag and harmonics associated with the voltage signal has been detected effectively and simultaneously; the sag has been localized with respect to the time range.

L. VOLTAGE SIGNAL WITH FLICKER AND HARMONICS

The voltage signal of a sine wave with superimposed flicker and 3^{rd}, 5^{th} & 7^{th} harmonics for a period of 10 cycles, PI and TLI plots are illustrated in Fig. 14. Fig. 14 (a) indicates the sine wave with superimposed harmonics and flicker with the regular pattern. Fig. 14 (b) indicates that there are ripples with the regular pattern observed over the entire time range of PI plot, which identifies the presence of harmonics. Further, the amplitude of the envelope evaluated by joining the peaks is changing in a regular pattern which detects the presence of flicker. The similar pattern is also observed in the Fig. 14 (c) where TLI plot also has ripples with the regular pattern over the entire time range, which identify the presence of harmonics. Further, the amplitude of the envelope evaluated by joining the peaks is changing in a regular pattern which detects the presence of flicker. Hence, multiple PQ disturbance of flicker and harmonics associated with the voltage signal has been detected effectively with the help of both the PI and TLI plots.

This article has been accepted for publication in a future issue of this journal, but has not been fully edited. Content may change prior to final publication. Citation information: DOI 10.1109/ACCESS.2020.3046425, IEEE Access

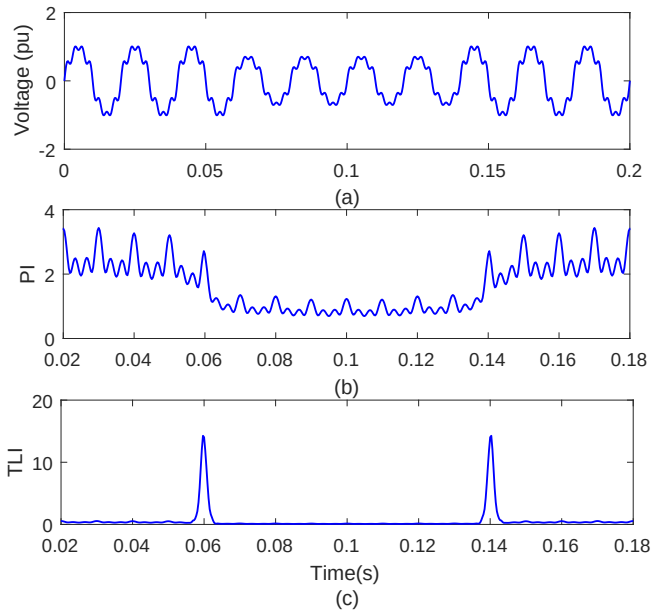

FIGURE 13. Voltage signal with sag and harmonics disturbance (a) voltage signal (b) power quality index (c) time location index

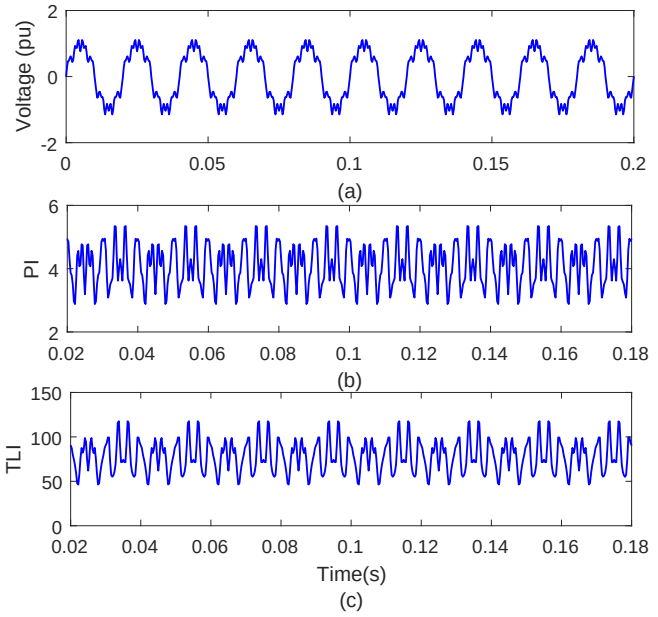

FIGURE 14. Voltage signal with flicker and harmonics disturbance (a) voltage signal (b) power quality index (c) time location index

M. VOLTAGE SIGNAL WITH FLICKER AND OSCILLATORY TRANSIENT

The voltage signal of a sine wave with superimposed flicker and OT ($0.08s$ to $0.10s$) for a period of 10 cycles, PI and TLI plots are illustrated in Fig. 15. Fig. 15 (a) indicates that the sine wave has a superimposed flicker with a regular pattern and an OT between $0.08s$ to $0.10s$. Fig. 15 (b) indicates that high magnitude has been observed between $0.08s$ to $0.10s$ with continuously increasing magnitude from $0.08s$ to $0.10s$ where the continuous pattern of ripples is available on the upper surface of the PI plot which indicates the presence of the OT. Further, a regular pattern of crest and trough with ripples superimposed on the crest over the entire time range indicates the presence of flicker. This specific pattern associated with the PI plot effectively detects the presence of multiple PQD comprising of an OT and a flicker. Fig. 15 (c) indicates that sharp magnitude peaks are associated with the TLI plot at $0.08s$ (incidence of OT) and $0.1s$ (end of OT) which help to effectively localize the OT. Hence, multiple PQ disturbance comprising of flicker and harmonics associated with the voltage signal has been detected effectively and simultaneously, the OT has been localized concerning the time range.

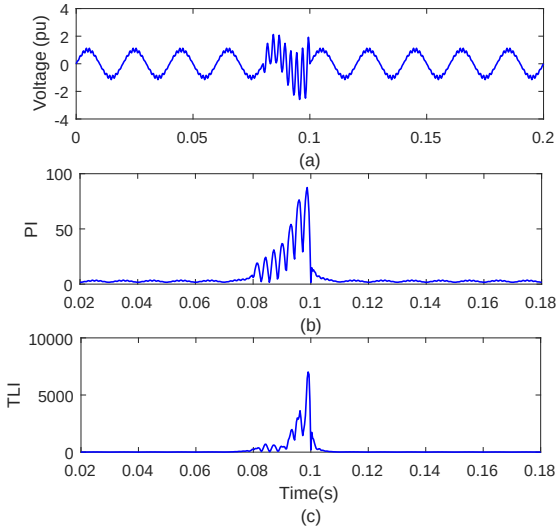

FIGURE 15. Voltage signal with flicker and oscillatory transient disturbance (a) voltage signal (b) power quality index (c) time location index

N. VOLTAGE SIGNAL WITH HARMONICS AND IMPULSIVE TRANSIENT

The voltage signal with superimposed multiple PQD of 3^{rd}, 5^{th} & 7^{th} harmonics and IT for a period of 10 cycles, PI and TLI plots are illustrated in Fig. 16. Fig. 16 (a) indicates that the sine wave has superimposed harmonics with a regular pattern and IT between $0.085s$ to $0.088s$. Fig. 16 (b) indicates that the sharp peak of very high magnitude has been observed between $0.085s$ to $0.088s$. This very high magnitude peak effectively detects the presence of IT superimposed on the signal. Further, there are ripples with the regular pattern over the entire time range, which effectively detects the harmonics associated with the voltage signal. Fig. 16 (c) indicates that there is a sharp peak of very high magnitude between $0.085s$ to $0.088s$, which helps to effectively detect and localize the IT. Hence, multiple PQ disturbance comprising of IT and harmonics associated with the voltage signal has been detected effectively and simultaneously the IT has been localized concerning the time range.

This article has been accepted for publication in a future issue of this journal, but has not been fully edited. Content may change prior to final publication. Citation information: DOI 10.1109/ACCESS.2020.3046425, IEEE Access

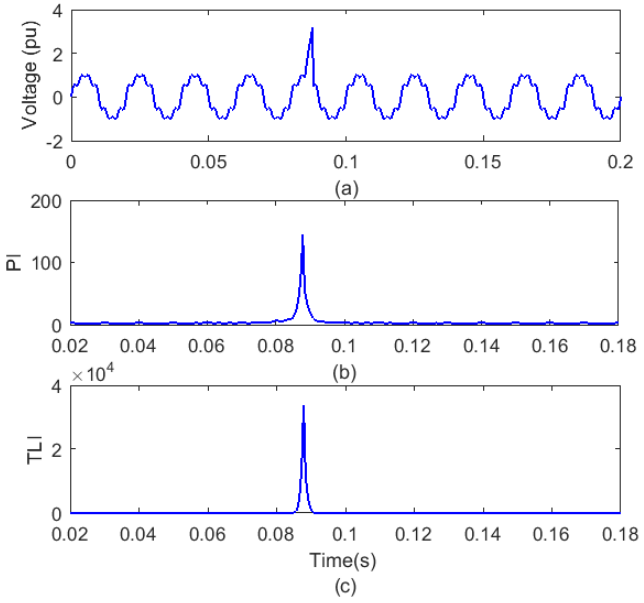

FIGURE 16. Voltage signal with harmonics and impulsive transient disturbance (a) voltage signal (b) power quality index (c) time location index

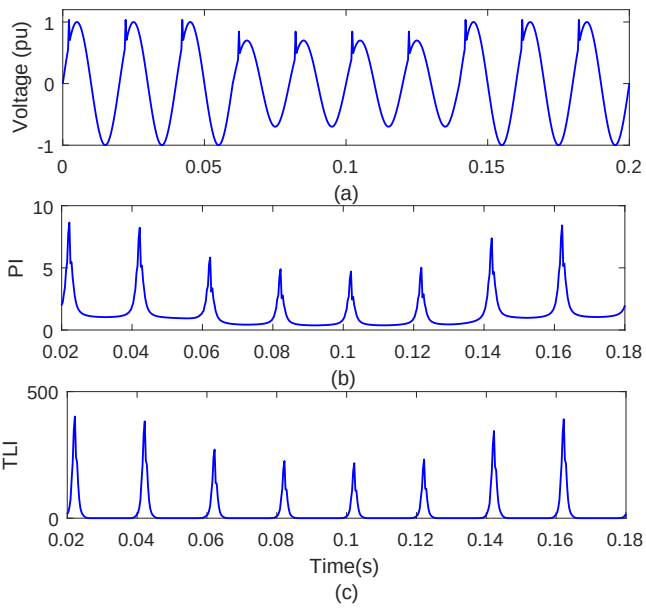

FIGURE 17. Voltage signal with spike and sag disturbance (a) voltage signal (b) power quality index (c) time location index

O. VOLTAGE SIGNAL WITH SPIKE AND SAG

The voltage signal of a sine wave with sag and MS for a period of 10 cycles, PI and TLI plots are illustrated in Fig. 17. Fig. 17 (a) indicates the sine wave with superimposed MS and MN with a regular pattern. Fig. 17 (b) indicates that a series of regularly spaced sharp peaks which have a single peak at the top surface are present where peak amplitude of the PI plot has decreased at $0.06s$ and again regains the original value at $0.14s$. This effectively detects the sag and MS associated with the voltage signal. Fig. 17 (c) also indicates the similar pattern of a series of regularly spaced sharp peaks with single peak present at the top surface and simultaneously the peak amplitude of the PI plot has decreased at $0.06s$ and again regains the original value at $0.14s$. However, rise and decay time for these peaks is lower compared to the peaks observed in the PI plot. Hence, multiple PQ disturbance comprising of spike and sag associated with the voltage signal has been detected effectively.

P. VOLTAGE SIGNAL WITH OSCILLATORY TRANSIENT, SAG, HARMONICS AND IMPULSIVE TRANSIENT

The voltage signal of a sine wave with a sag, an OT, 3^{rd}, 5^{th} & 7^{th} harmonics and IT for a period of 10 cycles, PI and TLI plots are illustrated in Fig. 18. Fig. 18 (a) indicates that sine wave has 3^{rd}, 5^{th} & 7^{th} harmonics with regular pattern, sag between $0.06s$ to $0.14s$, an OT between $0.08s$ to $0.10s$, and an IT between $0.022s$ to $0.025s$. Fig. 18 (b) indicates that amplitude of the PI plot has decreased at $0.10s$ and again regains the original value at $0.16s$ indicating the presence of sag. Fig. 18 (b) indicates that high magnitude has been observed between $0.08s$ to $0.10s$ with continuously increasing magnitude from $0.08s$ to $0.010s$ where the continuous pattern of ripples is available on the upper surface of the PI plot which indicates the presence of an OT. Fig. 18 (b) indicates that sharp peak of very high magnitude has been observed between $0.022s$ to $0.025s$ which effectively detects the presence of IT superimposed on the signal. Further, there are ripples with the regular pattern over the entire time range, which effectively detect the harmonics associated with the voltage signal. Fig. 18 (c) indicates that the TLI plot has sharp magnitude peaks at $0.06s$ (incidence of sag) and $0.14s$ (end of sag). These sharp magnitude peaks effectively localize the voltage sag. Fig. 18 (c) indicates that sharp magnitude peaks are associated with the TLI plot at $0.08s$ to $0.10s$, which helps to effectively localize the OT. Further, Fig. 18 (c) indicates that there is a sharp peak of very high magnitude between $0.022s$ to $0.025s$ which helps to detect and localize the IT effectively. Hence, multiple PQ disturbance comprising of sag, OT, harmonics and IT associated with the voltage signal has been recognized effectively.

Q. MISCELLANEOUS PQ DISTURBANCES

The proposed approach is also tested to recognize the DC offset and phase jump. It is observed that the algorithm effectively detects these disturbances. Further, the algorithm is based on the identification of deviation in the waveform from pure sinusoidal nature. Hence, it is adequate to recognize every disturbance associated with a waveform of voltage or current signals.

IV. RBDT BASED CLASSIFICATION OF PQDS

The features F5 to F8 defined in section II(c) are taken as input to the decision tree supported by rules for classifying the PQDs. Numerical values of these features utilized to design decision rules for classification of the investigated

This article has been accepted for publication in a future issue of this journal, but has not been fully edited. Content may change prior to final publication. Citation information: DOI 10.1109/ACCESS.2020.3046425, IEEE Access

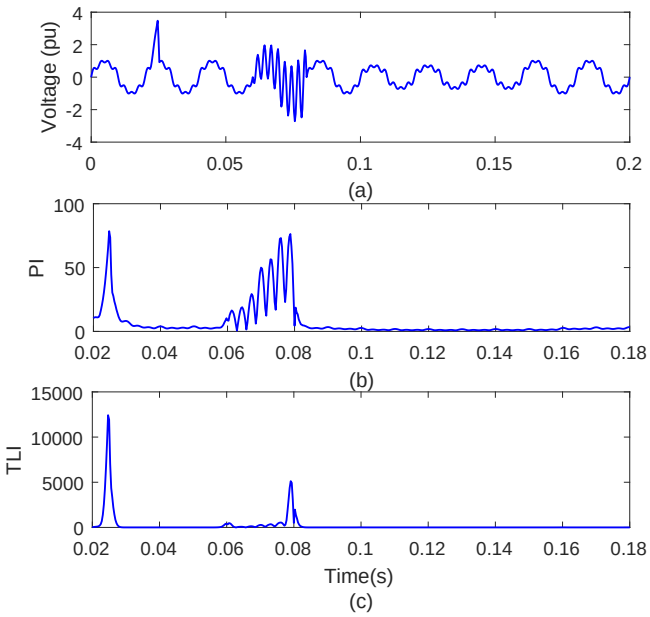

FIGURE 18. Voltage signal with oscillatory transient, sag, harmonics and impulsive Transient disturbance (a) voltage signal (b) power quality index (c) time location index

PQDs are provided in Table 3. These features are effective for recognizing the various characteristics of the PQDs. These are also effective to identify deviation of system voltage waveform from the nature of pure sine wave. Therefore, these features are effective in identifying the type of a PQD. Threshold magnitudes of features F5 to F8 to classify the PQDs using RBDT are decided after testing the algorithm for recognition of 100 data sets of each PQD computed by varying the parameters like magnitude, time of incidence of PQD, frequency of PQD, frequency of voltage signal (50 Hz and 60 Hz) and different levels of noise. Selected threshold magnitude for a feature will help for effective identification of all the PQDs. The feature F7 initializes the classification. The PQDs with F7>10^3 are included in the group PQ1, whereas the PQDs with F7<10^3 constitute the group PQ2.

PQ disturbances included in group PQ1 are further sub-classified using the values of feature F7. The PQDs having F7>10^6 constitute the group PQ11, whereas the PQDs with F7<10^6 are included in group PQ12. The disturbances included in group PQ11 are further classified using feature F6. The PQD14 (Voltage with harmonics) has values greater than 2, whereas the PQD7 (Voltage with IT) has valued less than 2. The PQDs included in group PQ12 are further sub-classified using the feature F5. The PQDs with F5>100 are included in group PQ121, whereas the PQDs with F5<100 are included in group PQ122. The disturbances included in the group PQ121 are further classified one by one. The PQD13 (voltage with flicker & OT) has F8>5. Subsequently, the PQD with F6>1.5 is PQD16 (voltage with OT, sag, harmonics & IT) and disturbance with F6<1.5 is PQD6 (Voltage with OT). The disturbances included in the group PQ122 are further classified one by one. The PQD9 (voltage with MN) has F8>2. Subsequently, the PQD with F5>2.25 is PQD10 (voltage with MS) and disturbance with F5<2.25 is PQD15 (voltage with MS & sag).

The PQ disturbances included in group PQ2 are further sub-classified using the feature F7. The PQDs having F7>50 constitute the group PQ21, whereas the PQDs with F7<50 are included in group PQ22. The disturbances included in the group PQ21 are further classified one by one. The PQD12 (voltage with flicker & harmonics) has F8>25. Subsequently, the PQD with F5>0.40 is PQD11 (voltage with sag & harmonics) and disturbance with F5<0.40 is PQD8 (Voltage with Harmonics). The PQ disturbances included in group PQ22 are further sub-classified using the feature F6. The PQDs having F6>1 constitute the group PQ221, whereas the PQDs with F6<1 are included in group PQ222. The disturbances included in the group PQ221 are further classified one by one. The PQD5 (voltage with flicker) has F7>5 whereas the PQD3 (voltage with swell) has F7<5. The disturbances included in the group PQ222 are further classified one by one. The PQD4 (voltage with MI) has F5>0.10. Subsequently, the PQD with F5>0.05 is PQD2 (voltage with sag) and disturbance with F5<0.05 is PQD1 which pure sine wave without any disturbance. Decisions supported by rules based classification of the PQDs are illustrated with the help of a flow chart in the Fig. 19, where the decision rules are also included for each step. Threshold magnitudes of features are decided by testing the algorithm on 100 data set of each PQ disturbance by changing the different parameters (refer Table 1 and 2).

V. PERFORMANCE EVALUATION

Performance of the algorithm for recognition of the PQDs supported by the features computed with the help of HT and ST is evaluated in terms of accurately classified and inaccurately classified PQDs (in numbers). The algorithm is tested for recognition of the PQDs, on 100 data set of each PQ disturbance with a noise level of 10dB SNR, and without noise. This data set is obtained by changing different parameters (refer Table 1 and 2). Table 4 demonstrates the performance of the algorithm in terms of accurately classified and inaccurately classified PQDs. It is established that algorithm is effective for recognition of the PQDs with very high accuracy which is greater than 99% in the absence of noise and greater than 98% with a noise level of 10 dB SNR superimposed on the voltage signals in addition to the PQD. The noise level of 10 dB SNR is the maximum noise level observed with the electrical signals. Hence, the proposed algorithm is effective to recognize the PQ disturbances even when the noise is variable between 10 dB SNR to 100 dB SNR.

Performance of algorithm is tested for recognition of wide range of different PQ disturbances. Results for recognition of voltage sag magnitude ranging from 20% to 80% are described in Fig. 20. Further, the values of features F5, F6, F7 and F8 for sag in voltage with 20%, 40%, 60% and 80% are detailed in Table 5. It is observed that sag in voltage for

TABLE 3. Numerical Values of Features Used as Input to the RBDT

Type of PQD	Features			
	F5	F6	F7	F8
PQD1	0.0076	0.9792	1.8477	1.5750×10^{-5}
PQD2	0.0940	0.9424	1.9076	1.5306×10^{-5}
PQD3	0.2619	1.2057	2.1229	4.3233×10^{-5}
PQD4	0.2357	0.8763	2.0403	1.4531×10^{-5}
PQD5	0.3073	2.6449	14.4868	9.0059
PQD6	126.3743	0.9977	2.0961×10^{5}	1.6270×10^{-5}
PQD7	104.3131	1.0563	4.9262×10^{6}	1.7197×10^{-5}
PQD8	0.2230	2.3715	108.1189	0.3574
PQD9	2.5229	1.6177	7.5000×10^{3}	7.6866
PQD10	2.6390	1.1562	6.8444×10^{3}	0.0177
PQD11	0.6684	2.0034	109.8587	0.3192
PQD12	0.4556	4.0774	347.7807	75.8061
PQD13	132.5229	2.7386	4.3855×10^{5}	12.1427
PQD14	88.4428	2.5211	4.1181×10^{6}	0.4138
PQD15	1.9798	1.0604	4.6300×10^{3}	0.0185
PQD16	154.9560	2.4435	9.7822×10^{5}	0.4253

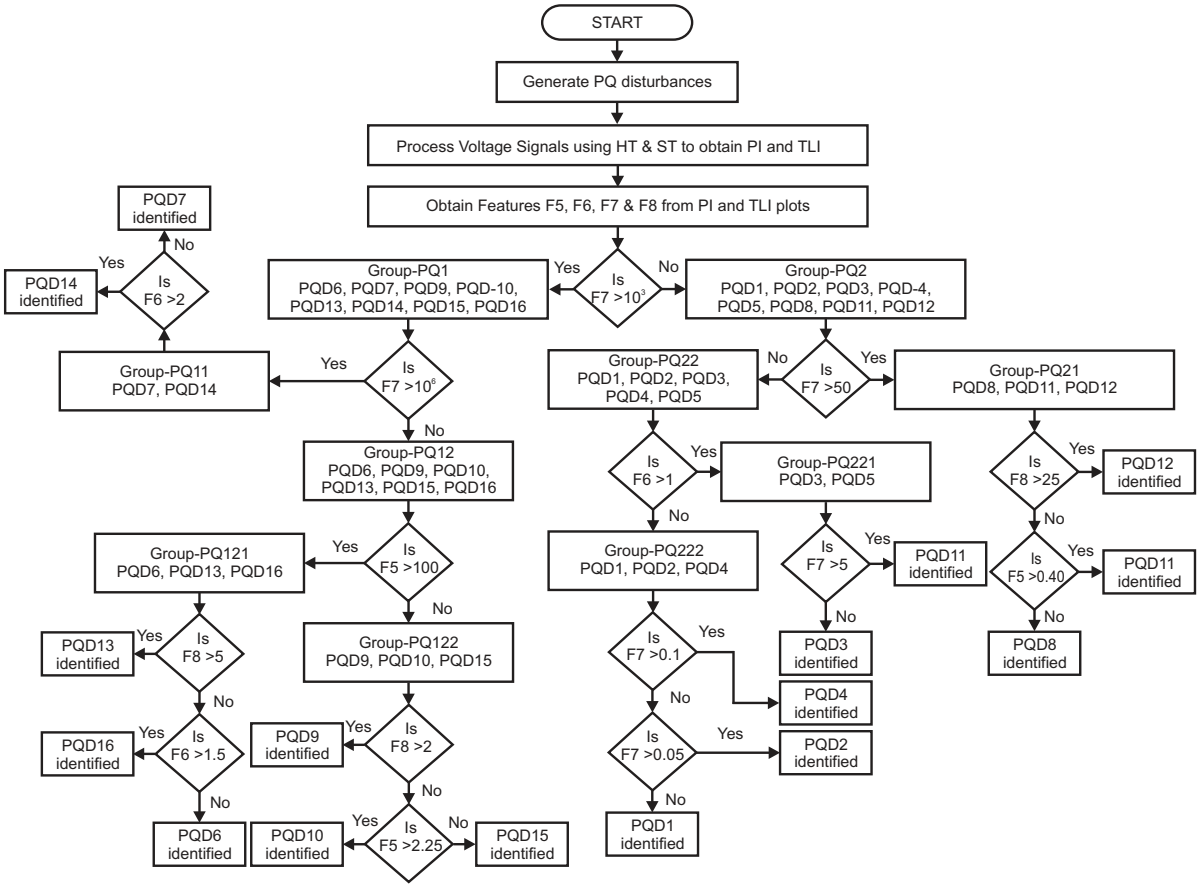

FIGURE 19. Decision rules and classification of PQDs

all possible range has been identified effectively and features F5 to F8 have values in the category of sag in voltage. Voltage sag with different range of magnitude have been classified in the category of voltage sag. Similar results are obtained for wide range of all the investigated PQ disturbances.

VI. VALIDATION OF ALGORITHM TO RECOGNIZE PQ DISTURBANCES IN PRACTICAL POWER SYSTEM NETWORK

The algorithm proposed for recognition of power quality disturbance is tested on a practical power system network of Rajasthan State of India reported in [23]. A brief description of the grid sub-stations (GSS) and transmission lines of the

This article has been accepted for publication in a future issue of this journal, but has not been fully edited. Content may change prior to final publication. Citation information: DOI 10.1109/ACCESS.2020.3046425, IEEE Access

TABLE 4. Performance of Algorithm for Recognition of PQDs

Type of PQD	Accurate PQDs (nos.)		Inaccurate PQDs (nos.)	
	Noise Absent	Noise (10dB SNR)	Noise Absent	Noise (10dB SNR)
PQD1	99	99	1	1
PQD2	99	99	1	1
PQD3	100	99	0	1
PQD4	100	100	0	0
PQD5	99	97	1	3
PQD6	100	100	0	0
PQD7	100	100	0	0
PQD8	100	97	0	3
PQD9	100	98	0	2
PQD10	100	99	0	1
PQD11	99	97	1	3
PQD12	99	98	1	2
PQD13	100	100	0	0
PQD14	100	99	0	1
PQD15	99	97	1	3
PQD16	100	100	0	0
Average efficiency	99.625%	98.81%		

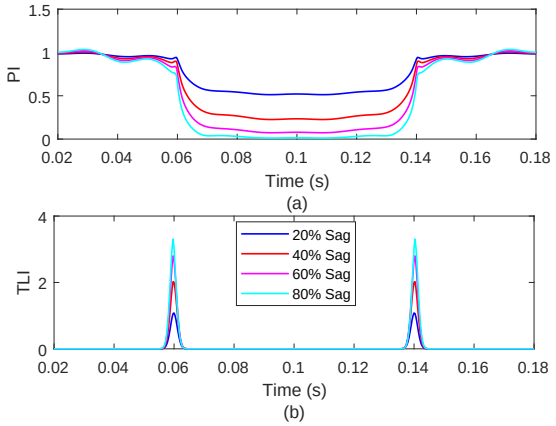

FIGURE 20. Performance of algorithm to recognize voltage sag of different magnitudes

TABLE 5. Numerical Values of Features Used as Input to the RBDT for Different Magnitudes of Voltage Sag

Voltage Sag (%)	Features			
	F5	F6	F7	F8
20%	0.0920	0.9480	1.8984	1.5378×10^{-5}
40%	0.09521	0.9322	1.9065	1.5288×10^{-5}
60%	0.09678	0.9125	1.9112	1.5232×10^{-5}
80%	0.09702	0.9022	1.9207	1.5208×10^{-5}

network is provided in Table 6. Generation contribution by the thermal power plants (TPP), power plants (PP) based on nuclear, hydro and renewable energy (RE) is detailed in Table 7 [24].

The network designed in the MiPower software and used for the planning and operational studies are considered for validation of the proposed PQ recognition algorithm and study is performed on 132 kV GSS Engineering College, Jodhpur. There are two 37.5/50 MVA, 132/33 kV transformers installed on this GSS to feed a load of the region. There

TABLE 6. Existing Grid Substation and Transmission Lines in Rajasthan

Voltage level (kV)	Number of Grid Sub-station	Total circuit length of lines (km)
765 kV	6	425.498
400 kV	27	7604.444
220 kV	124	15443.394
132 kV	459	18245.566
Total	616	41718.902

TABLE 7. Generation Contribution by Different Power Plants

Type of Power Plant	Capacity (MW)	Generation contribution (%)
Coal TPP	11918.45	56%
Gas TPP	824.60	4%
Nuclear PP	456.74	4%
Hydro PP	1961.95	9%
Wind Generation	3734.10	18%
Solar Generation	2178.10	10.29%
Biomass Generation	101.95	0.48%
Total	21175.90	100%

are total eight 33 kV outgoing distribution feeders emanating from this GSS which are feeding 11 MW (approximate) load to eight 33/11 kV GSS from where the load is supplied to the consumers. These outgoing feeders are designed in addition to the network already used for the planning purpose.

Faulty events are sources of voltage sag and transient disturbances in the network of the power system. A line to ground (LG) fault is simulated at time $0.1s$ at the middle of the first outgoing feeder which is 4.32 km long. The voltage signal recorded on the 33 kV bus of the 132 kV GSS Engineering College is recorded for a period of 10 cycles. This voltage signal is processed using the proposed algorithm to compute PI and TLI plots which are described in Fig. 21. Fig. 21 (a) indicates the recorded voltage signal for a period of $0.2s$. It is observed that due to the incidence of LG fault, the voltage magnitude decreases and fault transients are associated for the short time duration. Fig. 21 (b) indicates that amplitude of the PI plot has decreased at $0.1s$ indicating the presence of sag in voltage. Further, high magnitude available in the PI plot at the time of fault incidence indicates the presence of transients. Fig. 21 (c) indicates that TLI plot has sharp magnitude peak at the time of fault incidence. This is due to the combined effect of the initiation of the sag in voltage, and the presence of transient components. Hence, patterns of PI and TLI plots when combined together, effectively identify and localizes the sag in the practical network and also identify the transient components associated with the fault events. Further, the features F5, F6, F7 and F8 have values of 0.58, 1.98, 108.32, and 0.35, respectively. Hence, this disturbance is classified in the category of voltage sag and harmonic transients. Further, the algorithm is also successfully tested to identify the voltage swell due to switching on of a 2 MVAR capacitor bank.

This article has been accepted for publication in a future issue of this journal, but has not been fully edited. Content may change prior to final publication. Citation information: DOI 10.1109/ACCESS.2020.3046425, IEEE Access

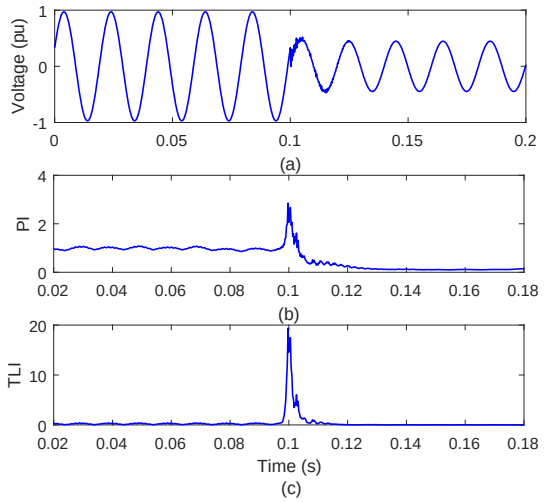

FIGURE 21. Voltage signal during event of LG fault (a) voltage signal (b) power quality index (c) time location index

VII. PERFORMANCE COMPARATIVE STUDY

Performance of the algorithm is compared with the Hilbert transform and Stockwell transform-based techniques reported in the literature. A technique using variance features extracted from the amplitude, median and kurtosis plots obtained by ST based decomposition of voltage signal with single-stage PQ and multiple PQ is reported in [12] and [13] respectively, where the classification of PQDs is achieved using the RBDT. This technique has the average efficiency of 97.033% and 96.67% for recognition of single-stage and multiple PQ disturbances, respectively. Further, a technique using variance features extracted using HT decomposition of voltage signal with single-stage PQ and multiple PQ is reported in [14] and [15], respectively, where the classification of PQDs is achieved using the RBDT. This technique has the average efficiency of 98.20% and 97.33% for recognition of single-stage and multiple PQ disturbances, respectively. The algorithm proposed in this paper has combined the Stockwell transform and Hilbert transform to improve performance of the PQ recognition, and average efficiency of 99.625% is achieved which is higher compared to the efficiency of algorithms reported in [12], [13], [14] and [15]. These papers have been considered for comparative study because waveforms of PQDs investigated in these papers are similar to that considered in this paper. Further, the algorithm based on ST and RBDT and reported in [17] has an average efficiency of 98.5% for recognition of single-stage PQ disturbance in the presence of noise level of 20dB SNR whereas the algorithm introduced in this paper has an efficiency of 98.81% in the presence of higher noise level of 10dB SNR. A comparative study indicating the performance of proposed algorithm and algorithm reported in [17] in noisy environment is detailed in Fig. 22. It is inferred that performance of proposed approach is superior compared to the approach reported in [17] during the noisy conditions. Hence, it is established that the proposed algorithm is more effective compared to the various techniques reported in the literature and can be used for the design of the online PQ monitoring devices for the utility grids.

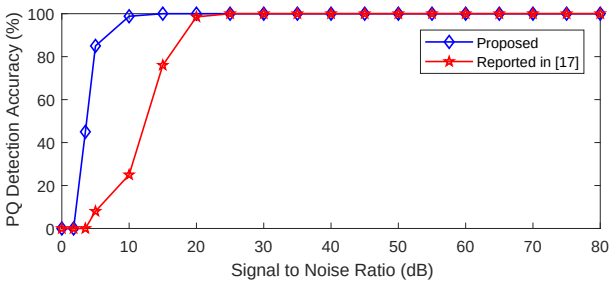

FIGURE 22. Comparative study for performance of algorithms in identification of voltage sag in noisy environment

The 640 samples of each investigated PQ disturbances are generated for comparing computational time of proposed approach with the method reported in [17]. A laptop of 64-bit operating system, 4 GB RAM, Intel(I) Core(TM)i5-3230M CPU@2.60 GHz processor is used to compute the computational time. The computational time involved in the computation of PI and TLI plots (detection of PQDs) is observed to be $0.256791s$, and computation time for classification of PQDs is $0.100326s$. Hence, the total computational time for detection and classification of a PQD using the proposed approach is $0.357117s$. Further, computational time involved in the computation of different ST based plots (detection of PQDs) is observed to be $1.8257s$, and computation time for classification of PQDs is $0.34561s$ using method reported in [17] which is based on ST and decision tree (DT) initialized Fuzzy C-means clustering (FCM). A comparative study of computational time of algorithm with algorithm based on ST+DT+FCM and reported in [17], using a bar chart is detailed in Fig. 23. Hence, it is established that proposed method is more faster compared to the many techniques reported in literature.

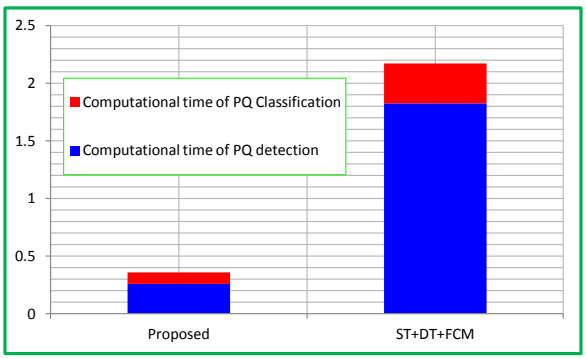

FIGURE 23. Computational time comparison

VIII. CONCLUSION

This paper introduced an algorithm based on the hybrid combination of features of voltage signals extracted using the

Hilbert transform and Stockwell transform for recognition of the PQ disturbances. Classification of the PQDs is achieved using rules supported by decisions using various features. Feature F1 computed using the HT and featured F2 to F4 computed using ST are used to obtain the PI and TLI plots. PQDs are identified by analysis of the patterns of these plots. Investigated single-stage PQDs include sag, swell, MI, IT, OT, flicker, harmonics, MS and MN. These PQDs are used to obtain the investigated multiple PQDs. The TLI plot is found to be effective in localization of the PQDs such as sag, swell, MI and OT. Features F5 to F8 are computed from the PI and TLI plots are considered as input to the RBDT for classification purpose. It is concluded that the proposed algorithm is effective for recognition of both the single-stage and multiple PQDs with an efficiency of 99.625%. Further, this algorithm is also effective to recognize both the single-stage and multiple PQDs with an efficiency of 98.81% in the presence of higher noise level of 10dB SNR. Performance of the algorithm is found to be superior compared to the algorithms based on the Stockwell transform and Hilbert transform reported in the kinds of literature. Proposed approach is faster and scalable to all range of voltages. The algorithm successfully recognized the PQDs associated with the practical utility network. This algorithm can be used to design online PQ monitoring devices which can be used to monitor PQ disturbances in the utility grids.

REFERENCES

[1] S. De and S. Debnath, "Real-time cross-correlation-based technique for detection and classification of power quality disturbances," IET Generation, Transmission Distribution, vol. 12, no. 3, pp. 688–695, 2018.

[2] G. D. J. Martinez-Figueroa, D. Morinigo-Sotelo, A. L. Zorita-Lamadrid, L. Morales-Velazquez, and R. D. J. Romero-Troncoso, "Fpga-based smart sensor for detection and classification of power quality disturbances using higher order statistics," IEEE Access, vol. 5, pp. 14 259–14 274, 2017.

[3] O. P. Mahela, A. G. Shaik, and N. Gupta, "A critical review of detection and classification of power quality events," Renewable and Sustainable Energy Reviews, vol. 41, pp. 495 – 505, 2015. [Online]. Available: http://www.sciencedirect.com/science/article/pii/S1364032114007564

[4] U. Singh and S. N. Singh, "A new optimal feature selection scheme for classification of power quality disturbances based on ant colony framework," Applied Soft Computing, vol. 74, pp. 216 – 225, 2019. [Online]. Available: http://www.sciencedirect.com/science/article/pii/S156849461830574X

[5] W. Lin, C. Wu, C. Lin, and F. Cheng, "Detection and classification of multiple power-quality disturbances with wavelet multiclass svm," IEEE Transactions on Power Delivery, vol. 23, no. 4, pp. 2575–2582, Oct 2008.

[6] R. Hooshmand and A. Enshaee, "Detection and classification of single and combined power quality disturbances using fuzzy systems oriented by particle swarm optimization algorithm," Electric Power Systems Research, vol. 80, no. 12, pp. 1552 – 1561, 2010. [Online]. Available: http://www.sciencedirect.com/science/article/pii/S037877961000163X

[7] O. P. Mahela, B. Khan, H. H. Alhelou, and S. Tanwar, "Assessment of power quality in the utility grid integrated with wind energy generation," IET Power Electronics, January 2020. [Online]. Available: https://digital-library.theiet.org/content/journals/10.1049/iet-pel.2019.1351

[8] T. Zhong, S. Zhang, G. Cai, and N. Huang, "Power-quality disturbance recognition based on time-frequency analysis and decision tree," IET Generation, Transmission Distribution, vol. 12, no. 18, pp. 4153–4162, 2018.

[9] T. Zhong, S. Zhang, G. Cai, Y. Li, B. Yang, and Y. Chen, "Power quality disturbance recognition based on multiresolution s-transform and decision tree," IEEE Access, vol. 7, pp. 88 380–88 392, 2019.

[10] L. Lin, D. Wang, S. Zhao, L. Chen, and N. Huang, "Power quality disturbance feature selection and pattern recognition based on image enhancement techniques," IEEE Access, vol. 7, pp. 67 889–67 904, 2019.

[11] G. S. Chawda, A. G. Shaik, O. P. Mahela, S. Padmanaban, and J. B. Holm-Nielsen, "Comprehensive review of distributed facts control algorithms for power quality enhancement in utility grid with renewable energy penetration," IEEE Access, pp. 1–22, 2020.

[12] M. Meena, O. P. Mahela, M. Kumar, and N. Kumar, "Detection and classification of power quality disturbances using stockwell transform and rule based decision tree," in 2018 International Conference on Smart Electric Drives and Power System (ICSEDPS), June 2018, pp. 227–232.

[13] ——, "Detection and classification of complex power quality disturbances using stockwell transform and rule based decision tree," in 2018 International Conference on Smart Electric Drives and Power System (ICSEDPS), June 2018, pp. 220–226.

[14] R. Saini, O. P. Mahela, and D. Sharma, "An algorithm based on hilbert transform and rule based decision tree classification of power quality disturbances," in 2018 IEEE 8th Power India International Conference (PIICON), Dec 2018, pp. 1–6.

[15] ——, "Detection and classification of complex power quality disturbances using hilbert transform and rule based decision tree," in 2018 IEEE 8th Power India International Conference (PIICON), Dec 2018, pp. 1–6.

[16] R. H. G. Tan and V. K. Ramachandaramurthy, "Numerical model framework of power quality events," European Journal of Scientific Research, vol. 43, no. 1, pp. 30–47, June 2010.

[17] O. P. Mahela and A. G. Shaik, "Recognition of power quality disturbances using s-transform based ruled decision tree and fuzzy c-means clustering classifiers," Applied Soft Computing, vol. 59, pp. 243 – 257, 2017. [Online]. Available: http://www.sciencedirect.com/science/article/pii/S1568494617303393

[18] I. Erdem, G. Asbjörnsson, and H. Kihlman, "Feedforward control for oscillatory signal tracking using hilbert transform," European Journal of Control, vol. 50, pp. 41 – 50, 2019. [Online]. Available: http://www.sciencedirect.com/science/article/pii/S0947358018305211

[19] R. G. Stockwell, L. Mansinha, and R. P. Lowe, "Localization of the complex spectrum: the s transform," IEEE Transactions on Signal Processing, vol. 44, no. 4, pp. 998–1001, April 1996.

[20] O. Mahela, B. Khan, H. Haes Alhelou, and P. Siano, "Power quality assessment and event detection in distribution network with wind energy penetration using stockwell transform and fuzzy clustering," IEEE Transactions on Industrial Informatics, pp. 1–1, 2020.

[21] O. P. Mahela and A. G. Shaik, "Power quality recognition in distribution system with solar energy penetration using s-transform and fuzzy c-means clustering," Renewable Energy, vol. 106, pp. 37 – 51, 2017. [Online]. Available: http://www.sciencedirect.com/science/article/pii/S0960148116311661

[22] K. Khalili-Damghani, F. Abdi, and S. Abolmakarem, "Hybrid soft computing approach based on clustering, rule mining, and decision tree analysis for customer segmentation problem: Real case of customer-centric industries," Applied Soft Computing, vol. 73, pp. 816 – 828, 2018. [Online]. Available: http://www.sciencedirect.com/science/article/pii/S1568494618305052

[23] S. R. Ola, A. Saraswat, S. K. Goyal, S. Jhajharia, B. Rathore, and O. P. Mahela, "Wigner distribution function and alienation coefficient-based transmission line protection scheme," IET Generation, Transmission Distribution, vol. 14, pp. 1842–1853, May 2020. [Online]. Available: https://digital-library.theiet.org/content/journals/10.1049/iet-gtd.2019.1414

[24] RVPN, in Rajasthan Rajya Vidyut Prasaran Nigam Ltd., Accessed on June 7, 2020. [Online]. Available: https://energy.rajasthan.gov.in/content/raj/energy-department/rajasthan-rajya-vidyut-prasaran-limited/en/about-us/power-map.html

RAJKUMAR KAUSHIK was born in Beswan, Aligarh, Uttar Pradesh, India, in 1990. He received his Bachelor of Technology degree from the B.S.A College of Engineering and Technology, Mathura, India, in 2012, and the Master of Technology degree from JIT Group of Institutions, Jaipur, India, in 2017, and pursuing his Ph.D. degree at Amity University Jaipur, India, all in electrical engineering. From 2017 he is working as an Assistant Professor with the Arya Institute of Engineering and Technology, Jaipur, India. His research interest includes power quality, optimization techniques and grid integration of renewable energy sources.

OM PRAKASH MAHELA was born in Sabalpura, Kuchaman City, Rajasthan, India, in 1977. He received the B.E. degree from the College of Technology and Engineering, Udaipur, India, in 2002, and the M.Tech. degree from Jagannath University, Jaipur, India, in 2013, and received the Ph.D. degree from Indian Institute of Technology Jodhpur, India, in 2018, all in electrical engineering. From 2002 to 2004, he was an Assistant Professor with the Rajasthan Institute of Engineering and Technology, Jaipur, India. From 2004 to 2014, he was a Junior Engineer with the Rajasthan Rajya Vidyut Prasaran Nigam Ltd., India and Assistant Engineer since July 20014. He has authored more than 150 research articles and book chapters. He performed more than 150 reviews for the prestigious journals of IEEE, Elsevier, Springer, Willey and Taylor & Francis. His research interest includes power quality, power system planning, grid integration of renewable energy sources, FACTS devices, transmission line protection, and condition monitoring. He was a recipient of the University rank certificate in 2002, Gold Medal in 2013, Best Research Paper Award in 2018 and C.V. Raman Gold Medal in 2019. He also received the certificates of outstanding contribution in the reviewing from Computer & Electrical Engineering, International Journal of Electrical Power & Energy Systems, Measurement, and Renewable & Sustainable Energy Reviews. He is a Senior Member of the IEEE.

PRAMOD KUMAR BHATT received his B.E. (EE) in 1993, M.E. (Power Electronics), in 2006 and Ph. D. in Electrical Engineering in 2018. For over 10 years he was extensively involved in industrial assignments, in particular R&D, system designing, modification, commissioning and maintenance. Systems automation such as PLC, SCADA, and power drives installation and testing. He is currently working as Associate Professor and coordinator Ph. D programme with the Amity School of Engineering and Technology (ASET), Jaipur, Rajasthan, India. His research interest includes Artificial Intelligence / Machine learning/ Soft Computing applications in smart grid power quality analysis and enhancement. Renewable energy integration challenges and opportunities in smart distribution / transmission system, smart microgrids, industrial microgrids and, condition monitoring of smart grid components.

BASEEM KHAN (M'16) received his Bachelor of Engineering degree in Electrical Engineering from Rajiv Gandhi Technological University, Bhopal, India in 2008. He received his Master of Technology and Doctor of Philosophy degrees in Electrical Engineering from the Maulana Azad National Institute of Technology, Bhopal, India, in 2010 and 2014, respectively. Currently, he is working as faculty member at Hawassa University, Ethiopia. His research interest includes power system restructuring, power system planning, smart grid technologies, meta-heuristic optimization techniques, reliability analysis of renewable energy system, power quality analysis and renewable energy integration. .

SANJEEVIKUMAR PADMANABAN (MEMBER'12SENIOR MEMBER'15, IEEE) received the PhD degree in electrical engineering from the University of Bologna, Bologna, Italy, in 2012. He was an Associate Professor with VIT University from 2012 to 2013. In 2013, he joined the National Institute of Technology, India, as a Faculty Member. In 2014, he was invited as a Visiting Researcher at the Department of Electrical Engineering, Qatar University, Doha, Qatar, funded by the Qatar National Research Foundation (Government of Qatar). He continued his research activities with the Dublin Institute of Technology, Dublin, Ireland, in 2014. Further, he served an Associate Professor with the Department of Electrical and Electronics Engineering, University of Johannesburg, Johannesburg, South Africa, from 2016 to 2018. Since 2018, he has been a Faculty Member with the Department of Energy Technology, Aalborg University, Esbjerg, Denmark. He has authored over 300 scientific papers. S. Padmanaban was the recipient of the Best Paper cum Most Excellence Research Paper Award from IET-SEISCON'13, IET-CEAT'16, IEEE-EECSI'19, IEEE-CENCON'19 and five best paper awards from ETAEERE'16 sponsored Lecture Notes in Electrical Engineering, Springer book. He is a Fellow of the Institution of Engineers, India, the Institution of Electronics and Telecommunication Engineers, India, and the Institution of Engineering and Technology, U.K. He is an Editor/Associate Editor/Editorial Board for refereed journals, in particular the IEEE SYSTEMS JOURNAL, IEEE Transaction on Industry Applications, IEEE ACCESS, IET Power Electronics, IET Electronics Letters, and Wiley-International Transactions on Electrical Energy Systems, Subject Editorial Board Member—Energy Sources—Energies Journal, MDPI, and the Subject Editor for the IET Renewable Power Generation, IET Generation, Transmission and Distribution, and FACTS journal (Canada).

FREDE BLAABJERG (Fellow, IEEE) received the Ph.D. degree in electrical engineering from Aalborg University, Aalborg, Denmark in 1995.

He was with ABB-Scandia, Randers, Denmark, from 1987 to 1988. He became an Assistant Professor in 1992, an Associate Professor in 1996, and a Full Professor of power electronics and drives in 1998. In 2017, he became a Villum Investigator. He is honoris causa with University Politehnica Timisoara (UPT), Romania and Tallinn Technical University (TTU) in Estonia. His current research interests include power electronics and its applications such as in wind turbines, PV systems, reliability, harmonics and adjustable speed drives. He has published more than 600 journal papers in the fields of power electronics and its applications. He is the co-author of four monographs and editor of ten books in power electronics and its applications.

Dr. Blaabjerg has received 32 IEEE Prize Paper Awards, the IEEE PELS Distinguished Service Award in 2009, the EPE-PEMC Council Award in 2010, the IEEE William E. Newell Power Electronics Award 2014, the Villum Kann Rasmussen Research Award 2014, the Global Energy Prize in 2019, and the IEEE Edison Medal in 2020. He was the Editor-in-Chief of the IEEE Transactions on Power Electronics from 2006 to 2012. He has been a Distinguished Lecturer for the IEEE Power Electronics Society from 2005 to 2007 and for the IEEE Industry Applications Society from 2010 to 2011 as well as from 2017 to 2018. In 2019–2020, he serves as the President of IEEE Power Electronics Society. He is the Vice-President of the Danish Academy of Technical Sciences too. He was nominated in 2014-2018 by Thomson Reuters to be between the most 250 cited researchers in Engineering in the world.